

Unravelling the Architecture of Membrane Proteins with Conditional Random Fields

Lior Lukov, Sanjay Chawla, Wei Liu, Brett Church, and Gaurav Pandey

University of Sydney, Australia

{lior.lukov, sanjay.chawla, bret.church}@sydney.edu.au,

University of Technology Sydney, Australia

Wei.Liu@uts.edu.au

University of Minnesota, USA

gaurav@cs.umn.edu

Abstract

In this paper we will show that the recently introduced graphical model: Conditional Random Fields (CRF) provides a template to integrate micro-level information about biological entities into a mathematical model to understand their macro-level behaviour. More specifically, we will apply the CRF model to an important classification problem in protein science, namely *the secondary structure prediction of proteins based on the observed primary structure*. A comparison on benchmark data sets against twenty eight other methods shows that not only does the CRF model lead to extremely accurate predictions but the modular nature of the model and the freedom to integrate disparate, overlapping and non-independent sources of information, makes the model an extremely versatile tool to potentially “solve” many other problems in bioinformatics. See the originally compiled PDF of this paper at: <https://drive.google.com/file/d/1IYF52Wk8m96KIlrQHUVtEBdm0Kw3M40c>

1 Introduction

An abundant and important class of proteins are the Integral Membrane Proteins (IMPs) which are found permanently embedded in the cell membrane. IMPs control a broad range of events essential to the proper functioning of cells, tissues and organisms including (i) the regulation of ion and metabolite fluxes, (ii) maintaining appropriate contact between cells, connective tissues, extracellular matrices and (iii) transducing extracellular signals to intracellular signalling pathways [5]. In addition, IMPs include families such as G-protein coupled receptors (GPCRs) that are the most common target of prescription drugs [34]. The task of determining a protein’s structure, especially

transmembrane segment prediction, has turned out to be difficult for IMPs [30, 22, 13]. The shortage of data on the structures of membrane proteins, compared to water soluble proteins, stems from a lack of success of X-ray crystallography and NMR spectroscopy on these proteins. Structural determination of IMPs can be problematic due to difficulties in obtaining sufficient amounts of sample. A further contributing factor is that IMPs are generally much more likely to become inactive while handling or waiting for crystallization [17].

Traditional transmembrane segment prediction methods are based on empirical observations that membrane regions are often 20 to 30 residues long, with high hydrophobicity around those regions and are connected with short loops containing positively charged residues. The methods vary in the way scoring metrics are assigned to the hydrophobicity property and the prediction algorithm. More recently, mathematical and probabilistic models such as neural networks [1] and hidden Markov models [13] have been applied to the transmembrane prediction problem. The most accurate methods claim to predict more than 90% of all membrane regions, with full helix prediction for all proteins higher than 80% [29].

However, as secondary data about of IMPs and amino acids has grown, an opportunity has arisen to integrate these diverse (but often correlated) sources of information towards improving transmembrane prediction. A new method is required which can seamlessly integrate information from heterogeneous sources and use it towards transmembrane prediction.

In this paper we show that the recently introduced graphical model, Conditional Random Field (CRF) provides such a framework to harmonize micro-level information about biological entities in order to understand their macro-level behavior. CRFs are related to Hidden Markov Models (HMMs) but are more general and do not place statistical restrictions on the type of information that can be integrated into the model [16]. For example, in HMMs an important assumption is that the observations (i.e., data) are independent of each other given their latent state (or label). This is a severe restriction and limits the type of information that can be integrated together [29].

More formally, the problem we address in this paper can be described as follows. Given a set of membrane protein sequences where each single record in the set contains a pair of sequences: the observation sequence consisting of amino acids represented by x , and the label sequence represented by y . The label sequence consists of indicators 1 or 0 which denote the presence or absence of the alpha-helix structure at that location. An example set of sequence pairs is shown in Fig 1. The objective of the secondary prediction problem is to predict the label sequence y given the observation sequence x .

Since CRFs provide a template for integrating information, our solution was to generate a large set of "indicators" (we call them features) and iteratively test the instantiated model against known standard benchmarks. Many of the features were derived using knowledge in the existing literature. To give one example about information integration, we were able to combine data about the hydrophobicity of amino acids and whether there are net electron donors or acceptors and test whether integrating these two pieces of information improves the predictability of the model. In the end we settled on a model which had an accuracy of 88% and 84% for segment and amino acid prediction respectively

which relates the two. Let x and y be observation and label sequence respectively. Our objective is to estimate the probability distribution $P(x, y)$. Without making any further assumptions, this estimation problem is intractable. For example, if the size of the observation alphabet is twenty and that of the label alphabet is two and all sequences are of fixed length n , then we need to estimate $20^n \times 2^n$ terms.

If the general problem is intractable, the question is what simplifying assumptions can be made on $P(x, y)$ in order to make the problem tractable without losing the essence of the relationship between x and y ?

At this point, it is best to relate $P(x, y)$ with an underlying graphical model. For the sequential classification problem, the graphical model is a pair of chains corresponding to the observation and the label sequence. The graphical model is used to encode and represent the factorization of $P(x, y)$. The nodes of the graph correspond to the random variables x and y , and two nodes are connected with an edge if the random variables are related or dependent. For example, suppose a sequence is of length n , then $x = x_1 x_2 \dots x_n$ is a sequence of random variables corresponding the amino acids. Similarly $y = y_1 y_2 \dots y_n$ corresponds to the sequence of secondary structure labels. If the x_i 's and y_j 's are related then that relationship is encoded in the underlying graph as an edge between the two nodes. Edges may be directed or undirected. Directed edges specify the direction of dependency between the two random variables.

For example in Fig 2(a), the factorization (known as Hidden Markov Model) is carried out as follows (See the originally compiled PDF of this paper at: <https://drive.google.com/file/d/1IYF52Wk8m96KIlrQHUVtEBdm0Kw3M40c>):

$$p(x, y) = p(y_1) p(x_1 | y_1) \prod_{i=2}^n p(y_i | y_{i-1}) p(x_i | y_i) \quad (1)$$

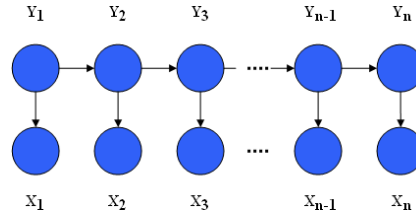
Similarly in Fig 2(b), a different factorization (known as Maximum Entropy Markov Model(MEMM)[19]) for $p(y|x)$ is encoded as:

$$p(y|x) = p(y_1 | x_1) \prod_{i=2}^n p(y_i | y_{i-1}, x_i) \quad (2)$$

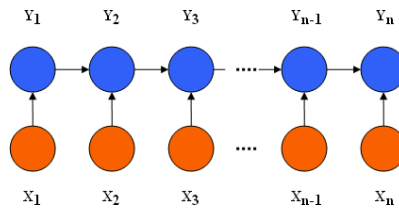
The pros and cons between the two factorizations has been a subject of intense debate in the data mining and machine learning literature and we refer the interested reader to some recent expositions and references therein [2, 26, 21]. However, we summarize the salient points:

1. Hidden Markov Models (HMMs) are *generative* while MEM models are *discriminative*. This means that HMMs have to make an assumption about how the observation is generated from the labels $P(x_i | y_i)$, while the MEM directly models the classification task and make an assumption on the functional form of $P(y_i | y_{i-1}, x_i)$ which is derived using the maximum entropy principle. The MEM functional form leads to an exponential model

$$p(y|x) = \frac{1}{Z(x, y)} \exp \left(\sum_j \lambda_j F_j(y, x) \right) \quad (3)$$



(a) HMM



(b) MEMM

Figure 2: Factorization of $P(x,y)$ is necessary in order to make the sequential classification problem tractable. Two common factorizations are the Hidden Markov Model (HMM) and the Maximum Entropy Markov Model (MEMM).

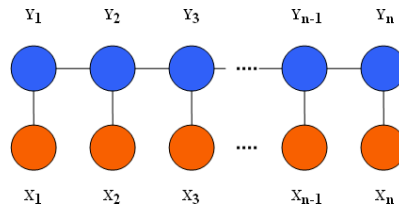


Figure 3: The CRF is an undirected graphical model. The Y_i are conditionally independent given their neighbors. Even though in the figure only X_i is connected to Y_i , the CRF model places no restrictions on the interactions between the Y and the X random variables.

1. The term $Z(x, y)$ is known as the normalization term (so that the probabilities add up to one) and because of the fact that it is dependent of both x and y it is called per-state normalization. The dependence of $Z(x, y)$ on both x and y leads to what is called *label-bias*[16]. The CRF model that we will derive will be very similar to the MEM model except that the underlying graphical model will be an undirected chain and the normalizing

term will be of the form $Z(x)$. (See the originally compiled PDF of this paper at: <https://drive.google.com/file/d/1IYF52Wk8m96KIlrQHUVtEBdm0Kw3M40c>)

$$p(y|x) = \frac{1}{Z(x)} \exp \left(\sum_j \lambda_j F_j(y, x) \right) \quad (4)$$

The label-bias problem occurs, for example, when $P(y_i | y_{i-1}, X) \approx P(y_i | y_{i-1})$. In this case, the MEM model completely ignores the information about the presence or absence of particular amino acids. However, the CRF model takes a more global view and does take the presence of amino acid into account.

2. Both HMMs and the MEM model assume that the label sequence is a markov chain, i.e., the state of the label at i , y_i is independent of all previous states except y_{i-1} .
3. For the observation sequence, HMMs assume that each observation is independent of all other observations given the labels. The MEM model does not make this assumption. In fact in the MEM model, the relationships between the observations and labels is mediated through the feature functions $F_j(x, y)$ and there are no limitations on the choice of the F_j 's. This flexibility allows micro-level biological information to be encoded into the MEM model without having to worry about observation independence. The CRF inherit this flexibility from the MEM model.

3 Feature Integration with the Model

The CRF model is a template which needs to be populated with problem dependent features. Features in our context represent function on the combination of the primary sequence and labels. It is helpful to think of features as micro-level information about membrane proteins. The role of the CRF model is to aggregate micro-level features in order to predict macro-level behaviour: namely, the secondary structure of the whole protein. Ideally features should be provided by domain-experts who are familiar with the micro-level behaviour of the entities under examination.

The number of different features which can be applied to a model is infinite. Assembling features which are relevant for the problem is an empirical process which involves many experiments. On each experiment, a combination of features is selected and then the model is evaluated based on its prediction. It is possible to evaluate and score the prediction based on the selected feature combination.

In this Section we present the different features which we have used in our experiments. To reiterate, features always appear as a combination of a particular label (state) and information about the observation sequence. We have selected a set of features to capture biological constraints and divided them into eighteen different groups

Table 1: Amino Acids Hydrophobic Index

Amino Acid	Hydrophobic Value	Amino Acid	Hydrophobic Value
Lysine (K)	-3.9	Proline (P)	-1.6
Arginine (R)	-4.5	Glycine (G)	-0.4
Histidine (H)	-3.2	Alanine (A)	1.8
Glutamic(E)	-3.5	Methionine (M)	1.9
Glutamine (Q)	-3.5	Cysteine (C)	2.5
Aspartic acid (D)	-3.5	Phenylalanine (A)	2.8
Asparagine (N)	-3.5	Leucine (L)	3.8
Trptophan (W)	-0.9	Valine (V)	4.2
Tyrosine (Y)	-1.3	Isoleucine (I)	4.5
Serine (S)	-0.8		
Threonine (T)	-0.7		

3.1 Features Extracted from Proteins Primary Structure

3.1.1 Start, End and Edge Features

By using these features we capture the probability of starting/ending a sequence with a given label or the transition probability for moving between the four combination of labels (H-H, H-NH, NH-H, NH-NH).

3.1.2 Basic Amino Acid Features

This feature captures the probability of amino acids to appear inside helical membranes. Twenty different unigram features exist of this type.

3.1.3 Hydrophobic Window Features

One of the most important physico-chemical characteristics of amino acids is hydrophobicity [31].

Hydrophobicity analysis has been shown to be an efficient way to detect transmembrane helices. Based on the work of Kyte and Doolittle [15], each amino acid is assigned a unique hydrophobic value. The values of the hydrophobic index are shown in Table 1.

For this feature a sliding window, consisting of 19 residues, is used to test if the average hydrophobic value of the 19 amino acids inside the window is greater than a certain threshold. 19 has been suggested to be the best number of amino acids in a sliding window [15]. In order to find the most effective threshold, 400 helix-segments and 400 loop-segments are randomly selected from the training dataset (The training dataset is introduced in section 4.1). We calculate and compare the average hydrophobic values for these two segments. As shown in Fig 4, most of the average hydrophobic values of helix-segments are greater than 1.0, while those of loop-segments are mostly lower than 1.0. Hence we use 1.0 as the threshold for this feature.

3.1.4 Hydrophilic Window Features

Similar to the Hydrophobic Window Features, the Hydrophilic Window Feature is used for detecting loop segments.

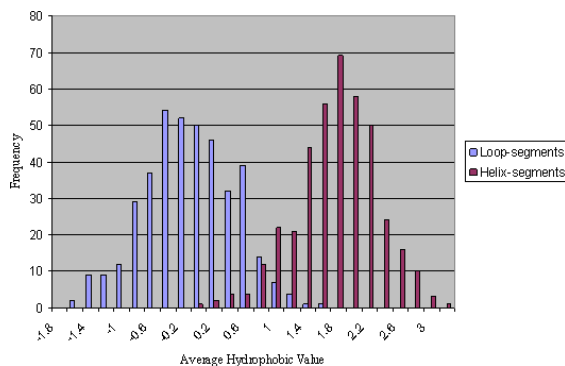


Figure 4: Comparison of Average Hydrophobic Values between Helix Segments and Nonhelix.

3.1.5 Single Side Neighboring Amino Acid Features

While the basic amino acid feature captures the tendency of a given amino acid to appear in a membrane helical structure, we are also interested in capturing the tendency of sequential combinations of amino acids to appear on the left or right of a particular label.

3.1.6 Single Side Shuffled Neighboring Amino Acid Features

Similar to Single Side Neighboring Amino Acid Features, but this time we are interested in capturing the tendency of the same amino acid given its adjacent neighbors without being concerned about their order. The motivation of creating the shuffled features is based on the hypothesis that the location of the transmembrane regions are determined by the difference in the amino acid distribution in various structural parts of the protein rather than by specific amino acid composition of these parts. We test this hypothesis in Section 4.3.2 by comparing the use of Single Side Neighboring Amino Acid Features vs. Single Side Shuffled Neighboring Amino Acid Features on a set of benchmark membrane helix sequences.

3.1.7 Single Side Hydrophobic Neighbouring Amino Acid Features

Similar to Single Side Shuffled Neighbouring Amino Acid Features, but this time we want to capture not only the composition of the adjacent amino acids, but also the hydrophobic tendency of these neighbouring residues. Since the hydrophobic value of a certain segment may affect the formation of a transmembrane helix [31], the hydrophobicity of neighbouring residues may also determine a single amino acid to be in a helix or not. We use the same “threshold” (1.0) as in Hydrophobic Values Window Features, so the Single Side Hydrophobic Neighbouring Amino Acid Feature is only active when the average hydrophobic

value of certain neighbouring residues is higher than 1.0.

3.1.8 Single Side Hydrophilic Neighbouring Amino Acid Features

Similar to the Hydrophobic Neighbouring Amino Acid Features, but this time we care about the neighbouring hydrophilic amino acids present in loop-segments. The same “threshold” is used here again, and the Single Side Hydrophilic Neighbouring Amino Acid Feature is only active when the average hydrophilic value of a certain number of neighbouring residues is lower than 1.0.

3.1.9 Double Side Neighboring Amino Acid Features

We have also captured the tendency of an amino acid to appear given its adjacent neighbors from both sides together.

3.1.10 Double Side Shuffled Neighboring Amino Acid Features

Similar to Double Side Neighboring Amino Acid Features, but this time we are interested in capturing the tendency of an amino acid to appear given adjacent neighbors from both sides together without being concerned about their order in which they appear.

3.1.11 Double Side Hydrophobic Neighbouring Amino Acid Features

Similar to Double Side Shuffled Neighbouring Amino Acid Features, but this time we want to capture not only the composition of the adjacent amino acids, but also the hydrophobic tendency of these neighbouring residues from both sides.

3.1.12 Double Side Hydrophilic Neighbouring Amino Acid Features

Similar to Double Side Hydrophobic Neighbouring Amino Acid Features, but this time we care about the hydrophilic amino acids present in **loop-segments**.

3.1.13 Amino Acid Property Features

Amino acids differ from one another in their chemical structure expressed by their side chains. The fact that amino acids from the same classification group appear in similar locations, motivated us to create special property features. We have adopted the classification from Sternberg [25], classifying the amino acids into nine groups¹, each group described by a unigram feature. Note that some amino acids may appear in more than one group simultaneously.

¹Aromatic (F,W,Y,H), Hydrophobic (M,I,L,V,A,G,F,W,Y,H,K,C), Positive (H,K,R), Polar (W,Y,C,H,K,R,E,D,S,Q,N,T), Charged (H,K,R,E,D), Negative (E,D), Aliphatic (I,L,V), Small (V,A,G,C,P,S,D,T,N), Tiny (A,G,S)

Table 2: Amino Acid Electronic Property

<i>ElectronicProperty</i>	<i>AminoAcids</i>
Strong donor	A, D, E, P
Weak donor	I, L, V
Neutral	C, G, H, S, W, M
Weak acceptor	F, Q, T, Y
Strong acceptor	K, N, R

The *Amino Acid Property Feature* highlights a very important fact: This feature and the basic unigram features are clearly dependent. For example, whenever the basic amino acid unigram feature corresponding to the amino acid F is active, the aromatic property feature will be active too (since F is classified as aromatic). Both these features are important. A Hidden Markov Model (HMM) cannot simultaneously handle both these features as it makes a strict assumption about independence between the observations (given the labels).

3.1.14 Border Features

By using these features we capture the border between a segment of amino acids labeled with one structure (helices/loops) and a segment labeled with another (loops/helices).

3.1.15 Short Loop Features

This feature aims at capturing the composition of short loops, which appear to be very difficult to predict especially when they are shorter than 7 residues [4]. In this feature we are not concerned about the order in which the amino acids appear. Instead, we capture the amino acids composition in the short loops. This feature is only active when the Amino Acid in a protein sequence is from a loop segment shorter than 7 residues.

3.1.16 Electron Transport Chain Features

Electron carriers and biochemical reactions are associated by electron transport chains, in which amino acids in protein sequences also take part [8]. The twenty amino acids are classified into five groups, as shown in Table 2, and are used in this feature to capture the influence of electron transport in helix formation.

3.1.17 Chemical Groups Features

Amino acids are characterized by their side chains. Based on the chemical compositions of the side chains, 18 new groups are defined, which form 36 new features, as shown in Table 3.

Table 3: Classification of Amino Acids by the Chemical Component in Their Side Chains

GroupNumber	ChemicalComponents	AminoAcids
1	--C--	R
2	=C ^{aromatic} --	Y, F, H, W
3	--CH--	L, V, I, T
4	--CH ₂ --	K, N, D, E, L, C, W, S, I, R, Q, F, H, Y
5	--CH ₂ ^{ring} --	P
6	--CH ₃	L, V, I, A, T, M
7	=CH ^{aromatic} --	W, F, Y, H
8	--CH ^{ring}	W, P
9	--C=O	N, Q
10	--COO--	D, E
11	=N--	H
12	--NH--	R
13	--NH ₂	N, R, Q
14	=NH ₂ ⁺	R
15	--NH ₃ ⁺	K
16	--OH	S, T, Y
17	--SH	C
18	--NH ^{ring} --	P, H, W

3.1.18 Sequence States Features

The sequence states mechanism in TMHMM [24, 13] have been adopted to be used as features. We divide protein sequences into three states: Helix Core (8 residues in the centre of a transmembrane helix segment), Helix Ends (5 residues at the ends of a transmembrane helix segment), Loops Ends (5 residues at the ends of a loop segment). This feature is based on the hypothesis that the differences between the amino acids distributions in the various structural parts are one of the driving forces in the formation of the transmembrane helices.

3.2 CRF Model Prediction Example

We now give a simple example of transmembrane helix prediction. For this example we will assume, for simplicity, that all proteins are 4 amino acids long, and the amino acids alphabet is composed of the amino acids $(A, C, D, E, F) \in \mathcal{X}$. The labelling alphabet describes if the current amino acid is inside a helix membrane/non-helix membrane region and denoted by $(0, 1) \in \mathcal{Y}$.

We define two property groups:

$$(A, C, F) \in \textit{Hydrophobic}$$

$$(C, D, E) \in \textit{Polar}$$

Note: the amino acid C is both Hydrophobic and Polar. We create the following unigram features:

$$u_n(x, i) = \begin{cases} 1 & \text{if the acid in sequence } x \\ & \text{at position } i \text{ is from type } n \\ 0 & \text{otherwise} \end{cases}$$

Table 4: Training Data in the Example

Observation	Labels
CAAF	0111
CDED	1000
DFAE	0110

Table 5: Activated features on a training set example

Feature Name	Occurences	Active on sequence
Basic Helix A	3	CAAF, DFAE
Basic Helix C	1	CDED
Basic Non-Helix C	1	CAAF
Basic Non-Helix D	3	CDED, DFAE
Basic Non-Helix E	2	CDED, DFAE
Basic Helix F	2	CAAF, DFAE
Hydrophobic Helix	6	CAAF, CDED, DFAE
Hydrophobic Non-Helix	1	CAAF
Polar Helix	1	CDED
Polar Non-Helix	6	CAAF, CDED, DFAE

$$u(x, i) = \begin{cases} 1 & \text{if the acid at position } i \text{ (A,C,F)} \\ 0 & \text{otherwise} \end{cases}$$

$$u(x, i) = \begin{cases} 1 & \text{if the acid at position } i \text{ (C,D,E)} \\ 0 & \text{otherwise} \end{cases}$$

Using these unigrams, each feature for describing the relationship between the observation and the two possible structures has the form:

$$f_{n_H}(y_i, x, i) = \begin{cases} u_n(x, i) & \text{if } y_i = \text{Helix membrane} \\ 0 & \text{otherwise} \end{cases}$$

$$f_{n_{NH}}(y_i, x, i) = \begin{cases} u_n(x, i) & \text{if } y_i = \text{Non-Helix membrane} \\ 0 & \text{otherwise} \end{cases}$$

We describe the relationship among the observation and the two possible structures, helix/non-helix membrane as a feature (as described in the previous Section).

We train the CRFs model using the training set as shown in Table ??.

Our goal is to predict the labels of the sequence *EAFD*. Table 5 shows the full list of activated features on the given training set.

In the training set a total of ten features are activated. Using maximum likelihood, the parameters $\lambda = (\lambda_1, \lambda_2, \dots, \lambda_{10})$ will be estimated. Table 6 shows the values of these feature parameters after they were calculated.

After calculating the feature parameters, the Viterbi algorithm is applied for labelling the test sequences. Now we will label the sequence *EAFD*. The first letter in the sequence, *E*, is a polar residue. From Table 6 we can calculate the total score of *E* by assigning it with a helical or a non-helical label. For assigning a helical label, the total score of *E* is *Polar Helix*, while for assigning a non-helical label, the total score is

Table 6: Trained feature parameters

Feature Name	Parameter value
Basic Helix A	1.7859
Basic Helix C	5.5170
Basic Non-Helix C	-5.5170
Basic Non-Helix D	1.7859
Basic Non-Helix E	1.5391
Basic Helix F	1.5391
Hydrophobic Helix	3.3251
Hydrophobic Non-Helix	-5.5170E-8
Polar Helix	5.5170E-8
Polar Non-Helix	3.3251

Table 7: Calculating the labels of the sequence *EAFD*

Letter	Label 0 score	Label 1 score	Final score	Assigned Label
<i>E</i>	4.8642	0	4.8642	0
<i>A</i>	4.8642	9.9752	9.9752	1
<i>F</i>	9.9752	14.8394	14.8394	1
<i>D</i>	19.9504	14.8394	19.9504	0

$Polar\ Non-Helix + Basic\ Non-Helix\ E = 4.8642$. Similarly, the total score of each one of the letters assembling the sequence *EAFD* is calculated for each label. Table 7 summarizes the steps of calculating the sequence labels.

Finally the algorithm assigns for each step these labels which yield the highest score. In this example *EAFD* is assigned with the predicted label sequence of *0110*.

4 Experiments, Evaluation and Analysis

In this section we report and analyze the results of three sets of experiments to test the CRF model for transmembrane prediction.

1. In the first experiment we compare different feature selection strategies and their effect on prediction accuracy. The CRF model with the best set of features was then evaluated against twenty eight models hosted at the “Static Benchmarking Server”(henceforth referred as the SBS) hosted at Columbia University [12].
2. In the second experiment we investigate the hypothesis that the location of the transmembrane region is determined by the distribution of amino acids in the region rather than their ordering. For example, if *FCD* is an observation sub-sequence then the probability that *FCD* is labelled as a transmembrane helix region is similar to the probability that the *permutation* of *FCD* is labelled as a transmembrane helix. This experiment also highlights the modular nature of feature integration into the CRF model. Biological hypothesis and information can be easily translated into features, integrated into the CRF model and tested.
3. The third experiment applies the CRF model on a large and well known

IMP complex, the Cytochrome C Oxidase. We compare our results against those reported, using “wet lab” experiments, by Wallin et. al. [33] and show that we are able to replicate many findings using the CRF-based data driven approach.

Before we describe the experiments, we briefly overview the data sets and the evaluation metrics used throughout this section.

4.1 Data Set

The CRF model was trained on a data set consisting of a set of benchmark sequences with experimentally confirmed transmembrane regions compiled by Möller et al. [20].² We have included only proteins with a high level of trust (assigned with transmembrane annotation trust level of A to C, as was suggested by Möller et al.). The resulting set consists of 148 transmembrane protein sequences with both helix and non-helix segments.

The model was tested on SBS [12]. This is a two-step process. First, a data set consisting of 2246 observation sequences was downloaded and labeled by the CRF model. Second, the labeled sequences were uploaded to the website which reported a comparative performance analysis with twenty eight other models. The experimental work flow is illustrated in Fig 5.

4.2 Prediction Metrics

The SBS uses two sets of metrics to compare models: per-residue and per-segment accuracy, which we now describe [5, 3].

4.2.1 Per-Residue Accuracy

In per-residue accuracy the predicted and actual labels are compared by residue. Let Ω_i be the sequence of residues in protein $i = 1, \dots, N_{prot}$. Furthermore, let $\omega_{(i,j)} \in \Omega_i$ be the residue in location j in sequence Ω_i . For simplicity, we denote $\omega_{(i,j)}$ as ω . Let³

$$y(\omega) = \begin{cases} 1 & \text{if } \omega \text{ is a TMH residue} \\ 0 & \text{if } \omega \text{ is a NTMH residue} \end{cases}$$

Similarly, let

$$\tilde{y}(\omega) = \begin{cases} 1 & \text{if } \omega \text{ is predicted as a TMH residue} \\ 0 & \text{if } \omega \text{ is predicted as a NTMH residue} \end{cases}$$

Table 8 lists the metrics which capture per-residue accuracy. The symbols in the last column are from Chen et al.[3], and are also used by SBS to report results.

²The data set can be accessed via <ftp://ftp.ebi.ac.uk/databases/testsets/transmembrane>

³TMH = Transmembrane Helix, NTMH = Non-Transmembrane Helix

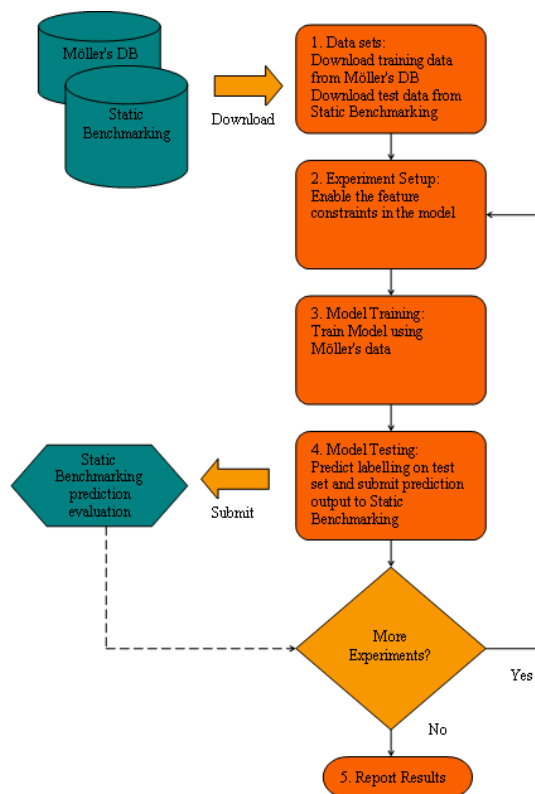


Figure 5: Transmembrane helix prediction experimental flow.

4.2.2 Per-Segment Accuracy

The per-residue accuracy measures ignore the sequential contiguity of the transmembrane helical (TMH) regions. We also want to determine how accurately a method correctly predicts the location of a TMH region.

In order to predict the sequential contiguity of the TMH region we have used the per-segment accuracy metric suggested by Chen et al. [3]. It requires a minimal overlap of **three residues** between the two corresponding segments and does not allow the same helix to be counted twice. For example consider the observed data and two possible prediction sequences: (0 = Non-Transmembrane Helix, 1 = Transmembrane Helix) as shown in Fig 6.

By using the per-segment metric, Prediction1 returns an accuracy of 100% (as it predicts two helices which are assigned with the two observation helices), while Prediction2 returns an accuracy of 50% (as it predicts one helix which is assigned only with the first observation helix). Table 8 also lists the metrics which capture per-segment accuracy.

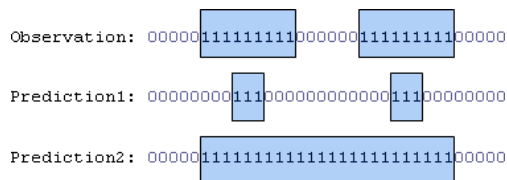


Figure 6: Per-segment accuracy example. Prediction1 is more accurate than Prediction 2 even though Prediction2 has a higher per-residue precision and recall.

Table 8: The metrics used to measure per-residue and per-segment accuracy. N_{prot} = Number of Proteins in the Data Set, TMH = Transmembrane Helix, NTMH = Non-Transmembrane Helix. [†] These symbols are from Chen et. al.

Per-Residue Metrics		
Description	Formula	Symbol [†]
TMH Recall	$P(\bar{y}(\omega) = 1 y(\omega) = 1)$	$Q_{2T}^{%obs}$
TMH Precision	$P(y(\omega) = 1 \bar{y}(\omega) = 1)$	$Q_{2T}^{%prd}$
NTMH Recall	$P(\bar{y}(\omega) = 0 y(\omega) = 0)$	$Q_{2N}^{%obs}$
NTMH Precision	$P(y(\omega) = 0 \bar{y}(\omega) = 0)$	$Q_{2N}^{%prd}$
Residues correctly predicted		Q_2
Per-Segment Metrics		
All observed TMH which are correctly predicted		$Q_{trmh}^{%obs}$
All predicted TMH which are correctly predicted		$Q_{trmh}^{%prd}$
Proteins for which all TMH are correctly predicted		Q_{ok}

4.3 Results and Analysis

4.3.1 Transmembrane Helix Prediction

The results of the CRF model, on the test set, in predicting the transmembrane helix (TMH) regions are shown in Fig 7. These results were obtained from SBS [12]. The six different feature combinations that were used are shown in Table 9. A detailed description of the feature sets used was given in Section 3.

As we can see from the result in Fig 7, there are three main kinds of features which contribute the most in capturing useful information from the training data: Hydrophobic-based features, neighbouring-acids-based features and sequence-state-based features.

After adding single and double side neighbouring features, Q_{ok} increases from 27% to 63% and Q_2 increases from 65% to 80%. After adding single and double shuffle neighbouring feature, Q_{ok} increases to 75%. After adding hydrophobic neighbouring features, Q_{ok} increases from 75% to 80% and Q_2 increases from 80% to 83%. Finally, after add sequence states features, Q_{ok} increases up to 88% and Q_2 increases up to 84%, and these are the best results

Table 9: Enabled and disabled feature combination.

Features	Exp 1	Exp 2	Exp 3	Exp 4	Exp 5	Exp 6	Exp 7	Exp 8
Basic	+	-	+	+	+	+	+	+
Properties	+	-	+	+	+	+	+	+
Hydrophobic Windows	-	-	+	+	+	+	+	+
Hydrophilic Windows	-	-	+	+	+	+	+	+
Single	-	+2	+5	+3	+5	+5	+5	+5
Double	-	+1	+1	+1	+3	+3	+3	+3
Single Shuffled	-	-	-	+3	+6	+6	+6	+6
Double Shuffled	-	-	-	+1	+3	+3	+3	+3
Single Hydrophobic	-	-	-	-	-	+3	+6	+6
Double Hydrophobic	-	-	-	-	-	+1	+3	+3
Single Hydrophilic	-	-	-	-	-	+3	+6	+6
Double Hydrophilic	-	-	-	-	-	+1	+3	+3
Border	-	-	-	-	-	-	+	+
Short Loops	-	-	-	-	-	-	+	+
Electronic	-	-	-	-	-	-	+	+
Groups	-	-	-	-	-	-	-	+
States	-	-	-	-	-	-	-	+

Basic = Basic Amino Acid Features, *Properties* = Amino Acid Property Features, *Hydrophobic Windows* = Hydrophobic Window Features, *Hydrophilic Windows* = Hydrophilic Window Features, *Single* = Single Side Neighboring Amino Acid Features (with 1 to 5 neighbors from left or right), *Double* = Double Side Neighboring Amino Acid Features (with 1 to 3 neighbors from both sides), *Single Shuffled* = Single Side Shuffled Neighboring Amino Acid Features (with 1 to 6 neighbors from left or right), *Double Shuffled* = Double Side Shuffled Neighboring Amino Acid Features (with 1 to 3 neighbors from both sides). *Single Hydrophobic* = Single Side Hydrophobic Neighbouring Amino Acid Features (with 1 to 6 neighbors from left or right), *Double Hydrophobic* = Double Side Hydrophobic Neighbouring Amino Acid Features (with 1 to 3 neighbors from both sides). *Single Hydrophilic* = Single Side Hydrophilic Neighbouring Amino Acid Features (with 1 to 6 neighbors from left or right), *Double Hydrophilic* = Double Side Hydrophilic Neighbouring Amino Acid Features (with 1 to 3 neighbors from both sides). *Border* = Border Features, *Short Loops* = Short Loop Features, *Electronic* = Electron Transport Chain Features, *Groups* = Chemical Group Features, *States* = Sequence States Features.

we have attained.

This suggests three rules of the micro-level behaviour of proteins:

1. Hydrophobic values of amino acids is a significant factor of locating helical segments [31];
2. The helical structure of amino acids is greatly influenced by its neighbours;
3. Differences between the amino acids distributions in the various structural parts are one of the driving forces in the formation of the transmembrane helices [24, 13].

Experiment 8 (henceforth referred as “the CRFs model”) outperforms the other experiments in most categories and was selected for comparison with other prediction models.

We submitted the result of the CRF model on the test data set to the SBS and obtained a comparative ranking against other available methods. This is shown in Table 10, and indicates that the CRF model performed the best both on per-segment and per-residue accuracy.



Figure 7: Accuracy of the eight Experiments based on Feature sets shown in Table 9

4.3.2 The Effect of Local Residue Distribution on Transmembrane Regions

We are interested in testing the hypothesis that the location of the transmembrane regions is determined by the composition of the amino acids in the transmembrane regions rather than their ordering. In order to test this hypothesis, we have carried out two experiments with different combinations of features turned on as shown in Table 11.

In Experiment 1 we have used single and double side neighboring amino acid features and in Experiment 2 we have used single and double side shuffled neighboring amino acid features (see Section 3 for an explanation of these features).

The prediction results of the two experiments are shown in Table 12 which suggest that the transmembrane helix regions are determined by the amino acid composition in the region rather than any specific ordering of the amino acids.

4.3.3 Cytochrome c oxidase Protein Analysis

The Cytochrome c oxidase protein has one of the most complex structures known to date with a total of 28 transmembrane helices [33]. A detailed wet lab analysis of this complex, in terms of residue distribution and amino acid properties has been reported by Wallin et al. [33] (henceforth referred as the observed results). We have replicated the results using the CRF model with the features defined

Table 10: Prediction score comparison between 29 methods.

Methods	Per-Segment			Per-Residue				
	Q_{ok}	$Q_{tmh}^{\%obs}$	$Q_{tmh}^{\%prd}$	Q_2	$Q_2^{\%obs}$	$Q_2^{\%prd}$	$Q_2^{\%obs}$	$Q_2^{\%prd}$
CRFs	88	99	98	84	80	90	88	80
PHDpsihtm08	84	99	98	80	76	83	86	80
HMMTOP2	83	99	99	80	69	89	88	71
DAS	79	99	96	72	48	94	96	62
TopPred2	75	90	90	77	64	83	90	69
TMHMM1	71	90	90	80	68	81	89	72
SOSUI	71	88	86	75	66	74	80	69
PHDhtm07	69	83	81	78	76	82	84	79
KD	65	94	89	67	79	66	52	67
PHDhtm08	64	77	76	78	76	82	84	79
GES	64	97	90	71	74	72	66	69
PRED-TMR	61	84	90	76	58	85	94	66
Ben-Tal	60	79	89	72	53	80	95	63
Eisenberg	58	95	89	69	77	68	57	68
Hopp-Woods	56	93	86	62	80	61	43	67
WW	54	95	91	71	71	72	67	67
Roseman	52	94	83	58	83	58	34	66
Av-Cid	52	93	83	60	83	58	39	72
Levitt	48	91	84	59	80	58	38	67
A-Cid	47	95	83	58	80	56	37	66
Heijne	45	93	82	61	85	58	34	64
Bull-Breese	45	92	82	55	85	55	27	66
Sweet	43	90	83	63	83	60	43	69
Radzicka	40	93	79	56	85	55	26	63
Nakashima	39	88	83	60	84	58	36	63
Fauchere	36	92	80	56	84	56	31	65
Lawson	33	86	79	55	84	54	27	63
EM	31	92	77	57	85	55	28	64
Wolfenden	28	43	62	62	28	56	97	56

Obtained from the “Static benchmarking of membrane helix predictions” server (sorted by Q_{ok})[12].

Table 11: The two different feature combinations used to test the effect of local residue distribution on TMH prediction.

Exp#.	Basic	Properties	Single	Double	Border	Active Features
1	+	+	+5	+3	-	803260
2	+	+	-	-	-	88594

in Experiment 8 (see Table 9).

We begin by predicting the distribution of individual residue type in the central membrane domain $\pm 10\text{\AA}$. The predicted and the observed results are shown in Fig 8(a) and indicate a high similarity between the observed and the predicted frequencies of the amino acids in the central membrane of the TMH regions.

Wallin et al. [33] also analyzed the frequency of the residues around the transmembrane helices based on the division of the amino acids into three groups: hydrophobic, polar and charged. We carried out a similar analysis using the CRF model and the results are shown in Fig 8(b). The concentration of hydrophobic residues around the central helix (± 13 residues around 0) is in the frequency range between 20 to 35% (average of 24%). It is interesting to note that the frequency distribution of the polar residues is a virtual mirror

Table 12: Transmembrane prediction results using two different feature combinations.

Per-Residue Methods	Per-Residue					Per-Segment		
	Q_2	$Q_{2T}^{\%obs}$	$Q_{2T}^{\%prd}$	$Q_{2N}^{\%obs}$	$Q_{2N}^{\%prd}$	Q_{ok}	$Q_{tmh}^{\%obs}$	$Q_{tmh}^{\%prd}$
1	83	72	84	93	78	75	87	91
2	83	75	86	89	77	75	92	83

Taken from the "Static benchmarking of membrane helix predictions" application written by Kernytsky et al. from University of Columbia, after submitting the prediction results of both experiments (sorted by Q_2) [12].

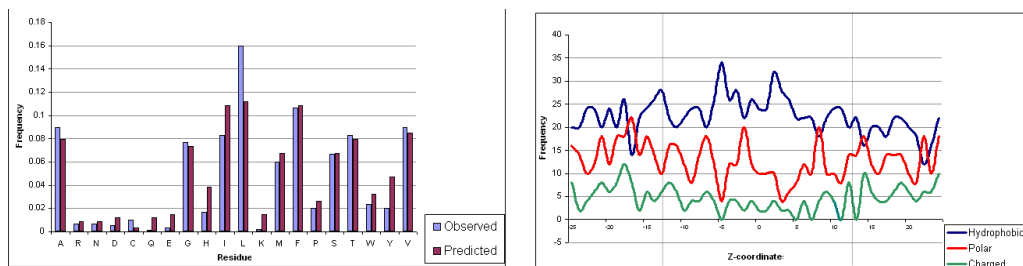
image of the hydrophobic frequency along the central helix (average of 11.5%). The charged residues tend to appear with an average frequency of 6% outside the helix membrane and 3.5% inside. These results are compatible with physical experiments which show that highly polar and charged amino acids are energetically unfavorable inside the membrane, with the hydrophobic core of the cell membrane filling between the polar head groups. Recent studies by Hessa et al. [10] using a biological assay of membrane segments insertion suggest that not only the degree of hydrophobicity is important in structuring transmembrane helices but also the energetic stability of the helices, defined by the sum of individual contribution from each amino acid. The authors have demonstrated that the contribution to the total apparent free energy depends strongly on the position of each residue within the helix [10]. Generally the more the polar and charged amino acids are close to the membrane center, the larger the energetic penalty generally is. The accepted explanation is that electrostatic forces close to the polar head group and beyond the membrane help to stabilize the polar and charged groups in amino acids.

In support of this conjecture, we predicted the tendency of arginine (both polar and charged residue) around the transmembrane helix. We found that the tendency of arginine favorable to be located outside the membrane as demonstrated in Fig 8(c).

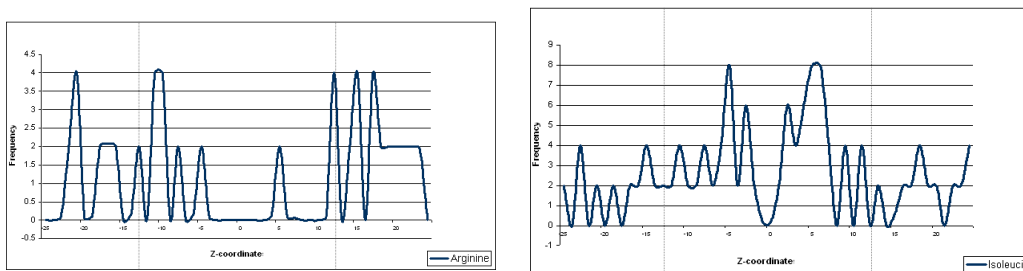
In contrast, we predicted the frequency around the membrane helix of isoleucine as an example of hydrophobic amino acids which according to observed experiments are favorable to appear in the center of the membrane. The results are demonstrated in Fig 8(d).

4.3.4 Approach

On the Cytochrome c oxidase experiments, we collected the distribution of individual residue type in the central membrane domain assuming that the central is on average 9 residues from the transmembrane border. In Wallin's work, he has calculated the distribution on a region of $\pm 10\text{\AA}$ [33], which we calculated using SwissPdbView [9], and found that on average the TMH region equals to 9 residues long. Wallin also referred his distribution figures to three different profiles: buried, intermediate and fully exposed residues. We compared our prediction results to the average values of the three profiles, since the sequence input that we used does not distinguish between these profiles.



(a) Residue frequencies in the central membrane $\pm 10\text{\AA}$ (b) Distribution of residues types in central membrane region $\pm 25\text{\AA}$



(c) Predicted Distribution of Arginine in TMH membranes $\pm 25\text{\AA}$ region. (d) Predicted Distribution of Isoleucine in the TMH membranes

Figure 8: Cytochrome C Oxidase analysis. The results obtained from the CRF model and those reported by Wallin et. al [7], using “wet lab” experiments show a striking similarity. The distribution of Isoleucine and Arginine are consistent with the explanation by Hessa et. al[27]

The CRFs model was trained using data set consists of a set of benchmark sequences with experimentally confirmed transmembrane regions, which are significantly different, based on pairwise similarity clustering [20]. All occurrences of Cytochrome c oxidase sequences were removed from the training set to assure that the training set and test set are not overlapping.

5 Conclusions

Conditional Random Fields (CRF) are a class of statistical models which can be used to integrate disparate, overlapping and non-independent micro-level information to make predictions at the macro-level. In this paper we have applied the CRF model to predict the secondary structure of membrane proteins on the basis of their primary structure. Comparisons against twenty eight other models shown that the results of the CRF model are extremely accurate. We have also compared results of the CRF model against those obtained from wet

lab experiments and have shown that we can replicate many of the important findings with striking accuracy. More importantly, the modular nature makes it possible for biologists to rapidly integrate and test new features (experiments), for relevance, in a mathematical model. The CRF model is extremely versatile and its use in bioinformatics is very likely to grow.

References

- [1] Somashekar Akkaladevi and Ajay K Katangur. Protein secondary structure prediction using bayesian inference method on decision fusion algorithms. *Parallel and Distributed Processing Symposium*, pages 1–8, 2007.
- [2] C. Bishop. *Pattern Recognition and Machine Learning*. Springer, 2006.
- [3] Chien Peter Chen, Andrew Kernytsky, and Burkhard Rost. Transmembrane helix predictions revisited. *Protein Science*, 11:2774–2791, 2002.
- [4] Chien Peter Chen and Burkhard Rost. Long membrane helices and short loops predicted less accurately. *Protein Science*, 11:2766–2773, 2002.
- [5] Chien Peter Chen and Burkhard Rost. State-of-the-art in membrane protein prediction. *Applied Bioinformatics*, 1:21–35, 2002.
- [6] Trevor Cohn. Efficient inference in large conditional random fields. In *ECML*, pages 606–613, 2006.
- [7] Miklos Cserzo, Erik Wallin, Istvan Simon, Gunnar von Heijne, and Arne Elofsson. Prediction of transmembrane alpha-helices in prokaryotic membrane proteins: the dense alignment surface method. *Protein Engineering*, 10(6):673–676, 1997.
- [8] Madhavi K. Ganapathiraju. Application of language technologies in biology: Feature extraction and modeling for transmembrane helix prediction. *Unpublished, PHD thesis*, 2007.
- [9] N. Guex and M.C. Peitsch. Swiss-model and the swiss-pdbviewer: An environment for comparative protein modeling. *Electrophoresis*, 18:2714–2723, 1997. <http://www.expasy.org/spdbv/>.
- [10] Tara Hessa, Hyun Kim, Karl Bihlmar, Carolina Lundin, Jorrit Boekel, Helena Andersson, IngMarie Nilsson, Stephen H. White, and Gunnar von Heijne. Recognition of transmembrane helices by the endoplasmic reticulum translocon. *Nature*, 433:377–381, 2005.
- [11] Wolfgang Hoschek. The colt distribution: Open source libraries for high performance scientific and technical computing in java, August 2005. <http://hoschek.home.cern.ch/hoschek/colt/>.

- [12] Andrew Kernytsky and Burkhard Rost. Static benchmarking of membrane helix predictions. *Nucl Acids Res*, 31 In press., 2003. <http://cubic.bioc.columbia.edu/cgi-bin/var/kernytsky/tmh/advanced-process.cgi>.
- [13] Anders Krogh, Bjorn Larsson, Gunnar von Heijine, and Erik L.L. Sonnhammer. Predicting transmembrane protein topology with a hidden markov model: Application to complete genomes. *Journal of Molecular Biology*, 305:567–580, 2001.
- [14] Sanjiv Kumar and Martial Hebert. Discriminative random fields. *International Journal of Computer Vision*, 68(2):179–201, 2006.
- [15] J. Kyte and R. F. Doolittle. A simple method for displaying the hydropathic character of a protein. *J Mol Biol*, 157(1):105–132, May 1982.
- [16] John Lafferty, Andrew McCallum, and Fernando Pereira. Conditional random fields: Probabilistic models for segmenting and labeling sequence data. In *Proc. 18th International Conf. on Machine Learning*, pages 282–289. Morgan Kaufmann, San Francisco, CA, 2001.
- [17] J. F. Leite, A. A. Amoscato, and M. Cascio. Coupled proteolytic and mass spectrometry studies indicate a novel topology for the glycine receptor. *Biol. Chem.*, 275:13683–13689, 2000.
- [18] Robert Malouf. A comparison of algorithms for maximum entropy parameter estimation. pages 1–7, Morristown, NJ, USA, 2002. Association for Computational Linguistics.
- [19] Andrew McCallum, Dayne Freitag, and Fernando C. N. Pereira. Maximum entropy markov models for information extraction and segmentation. In *ICML*, pages 591–598, 2000.
- [20] Steffen Moller, Evgenia V. Kriventseva, and Rolf Apweiler. A collection of well characterized integral membrane proteins. *Bioinformatics*, 16:1159–1160, 2000.
- [21] Andrew Y. Ng and Michael I. Jordan. On discriminative vs. generative classifiers: A comparison of logistic regression and naive bayes. In *NIPS*, pages 841–848, 2001.
- [22] Dariusz Przybylski and Burkhard Rost. Alignments grow, secondary structure prediction improves. *PROTEINS: Structure, Function, and Genetics*, pages 197–205, 2002.
- [23] L.R. Rabiner. A tutorial on hidden markov models and selected applications in speech recognition. volume 77, pages 257–285. IEEE, 1989.
- [24] Erik L.L. Sonnhammer, Gunnar von Heijine, and Anders Krogh. A hidden markov model for predicting transmembrane helices in protein sequences. *Proceedings of ISMB 6*, pages 175–182, 1998.

- [25] Michael J.E. Sternberg. *Protein Structure Prediction: A Practical Approach*. Oxford University Press, 1996.
- [26] Charles Sutton and Andrew McCallum. An introduction to conditional random fields for relational learning. In Lise Getoor and Ben Taskar, editors, *Introduction to Statistical Relational Learning*. MIT Press, 2006.
- [27] Hessa T., S.H. White, and G. von Heijne. Membrane insertion of a potassium-channel voltage sensor. *Science*, 307:307, 2005.
- [28] T. Tsukihara, H. Aoyama, E. Yamashita, T. Tomizaki, H. Yamaguchi, K. Shinzawa-Itoh, R. Nakashima, R. Yaono, and S. Yoshikawa. Structures of metal sites of oxidised bovine heart cytochrome c oxidase at 2.8 Å. *Science*, 269:1069–1074, 1995.
- [29] Gabor E. Tusnady and Istvan Simon. Principles governing amino acid composition of integral membrane proteins: Application to topology prediction. *Journal of Molecular Biology*, pages 498–506, 1998.
- [30] Gabor E. Tusnady and Istvan Simon. The hmmtop transmembrane topology prediction server. *Bioinformatics Application Note*, 17(9):849–850, 2001.
- [31] Gunnar von Heijne. Membrane protein structure prediction: Hydrophobicity analysis and the positive-inside rule. *Journal of Molecular Biology*, 225:487–494, 1992.
- [32] Hanna M. Wallach. Efficient training of conditional random fields. Master’s thesis, University of Edinburgh, 2002.
- [33] Erik Wallin, Tomitake Tsukihara, Shinya Yoshikawa, Gunnar von Heijne, and Arne Elofsson. Architecture of helix bundle membrane proteins: An analysis of cytochrome c oxidase from bovine mitochondria. *Protein Science*, 6:808–815, 1997.
- [34] A. Wise, K. Gearing, and S. Rees. Target validation of g-protein coupled receptors. *Drug discovery today*, 7:235–246, 2002.

6 Appendix 1: CRF Definition and Model Derivation

Here we derive the CRF model in detail. A CRF model is an undirected markov model and the resulting probability distribution is equivalent to a conditional Gibbs distribution [16, 14].

Let $G = (V, E)$ be a graph, $Y = (Y_v)_{v \in V}$ be a family of finite-valued random variables, and $X = (X_v)_{v \in V}$ be a family of real-valued functions.

Definition 1 (Y, X) is a conditional random field (CRF) if

1. $P(Y|X) > 0 \forall Y$

2. For all $v \in V$

$$P(Y_v|Y_{V-v}, X) = P(Y_v|Y_{N(v)}, X)$$

where $N(v)$ are the neighbors of v in G . This is called the Markov property.

Definition 2 Y is a Gibbs field if

$$P(Y) = \frac{1}{Z} \exp \left(- \frac{1}{T} U(Y) \right)$$

where Z is a normalizing constant, T is a constant called the temperature (which we assume is equal to one), and U is called the energy which can be expressed as:

$$U(Y) = \sum_{c \in C} U_c(Y)$$

where C is the set of all cliques (completely connected subgraphs) in G , and U_c is the energy for a particular clique.

According to the Hammersley-Clifford Theorem, a CRF is equivalent to a Gibbs field, thus

$$P(Y|X) \propto \exp\{U(Y, X)\} = \exp\left\{ \sum_{c \in C} U_c(Y, X) \right\}^4 \quad (5)$$

For sequential data, the graph G is a chain and therefore the clique set C consists of vertices (C_1) and edges (C_2), thus

$$U(Y, X) = \sum_{\{v\} \in C_1} V_1(Y_v, X) + \sum_{\{v, w\} \in C_2} V_2(Y_v, Y_w, X)$$

Using the notation of Lafferty [16] we can re-write Equation (5) as: \square

$$p_\theta(y|x) \propto \exp \left[\sum_{e \in E, j} \lambda_j f_j(e, y|_e, x) + \sum_{v \in V, j} \mu_j g_j(v, y|_v, x) \right]$$

where x is a data sequence, y a label sequence, $y|_S$ is the set of components of y associated with the vertices in subgraph S . The vectors f and g represent the local features with corresponding weight vectors λ and μ .

The joint distribution can be expressed in a slightly different form: \square

$$p_\theta(y|x) \propto \exp \left[\sum_{i, j} \lambda_j f_j(y_{i-1}, y_i, x, i) + \sum_{i, k} \mu_k g_k(y_i, x, i) \right] \quad (6)$$

$f_j(y_{i-1}, y_i, x, i)$ is a transition feature function of the entire observation sequence and the labels at positions i and $i-1$ in the label sequence. $g_k(y_i, x, i)$ is a state feature function of the entire observation sequence and the label at position i in the label sequence. $\theta = (\lambda_j, \mu_k)$ is estimated from the training data. We assume that the feature functions f_k and g_k are given and fixed [32]. The features serve as a “gateway” of incorporating biological information into the model.

⁴The minus sign has been absorbed in the function.

6.1 Feature Functions and Model Estimation

The feature functions constrain the conditional probability distribution $p(y|x)$. The satisfaction of a constraint increases the likelihood of the global configuration. Note that no feature independence assumption is made, and several dependent overlapping features are allowed. Different weights assigned to the parameters associated with the features, can be used to distinguish between important and irrelevant features.

An example of a feature is:

$$u(x, i) = \begin{cases} 1 & \text{if the amino acid at position } i \text{ is polar} \\ 0 & \text{otherwise} \end{cases}$$

An example of how the $u(x, i)$ feature is combined with possible state (label) information is as follows. If the current state in a state function, or the current and previous state in a transition function are satisfied then the feature function takes on the value $u(x, i)$ [32]. For example, the feature function $f_j(y_{i-1}, y_i, x, i)$ is assigned with the return value of the function $u(x, i)$, in case that the label at position $i - 1$ and i correspond to the α -helix structure,

$$f_j(y_{i-1}, y_i, x, i) = \begin{cases} u(x, i) & \text{if } y_{i-1} = \alpha \text{ helix and} \\ & y_i = \alpha \text{ helix} \\ 0 & \text{otherwise} \end{cases}$$

In what follows, we generalize the transition functions to include state functions by writing:

$$g(y_i, x, i) = f(y_{i-1}, y_i, x, i)$$

We also define the sum of a feature over the sequence by:

$$f_j(x, y) = \sum_{i=1}^n f_j(y_{i-1}, y_i, x, i)$$

where $f_j(y_{i-1}, y_i, x, i)$ refers to either transition or state function [32]. Therefore, the probability of a label sequence y given the observation sequence x is of the form:

$$p_\lambda(y|x) = \frac{1}{Z_\lambda(x)} \exp\left(\sum_j \lambda_j f_j(x, y)\right) \quad (7)$$

where

$$Z_\lambda(x) = \sum_y \exp\left(\sum_j \lambda_j f_j(x, y)\right) \quad (8)$$

Equation 7 is the ‘‘closed-form’’ of the CRF model and it is important to note that it is normalized over the whole observation sequence x .

A function $L_p(\lambda)$ continues to remain concave because $L_p(\lambda)$ is concave and so is $-\frac{\lambda_j^2}{2\sigma^2}$ and the sum of concave functions is concave. The σ^2 is a free parameter and large value of σ^2 corresponds to a higher penalty for larger λ_j terms. However, as noted by Sutton et. al.[26] past research has shown that the final estimated λ seems to be only moderately sensitive to the choice of σ^2 .

6.2 Complete Algorithm: Parameter Estimation, Labeling and Complexity

The complete outline of the algorithm which calculates the maximum likelihood using the training data and then labels test sequences is shown in Algorithm 1. We walk through the steps and also note the computational complexity wherever relevant.

Algorithm 1 Parameter Estimation and Labeling

- 1: Initialize
 - $\lambda = \langle \lambda_j \rangle_{j=1}^K$ {the feature parameters}
 - E {convergence criterion for λ }
 - σ^2 {regularization parameter for M_{λ} }
 - 2: **Maximum Likelihood Estimation Phase:**
 - 3: For each active feature f_j , calculate $\sum_{x,y} \tilde{p}(x,y) f_j(x,y)$ from training data
 - 4: **while** convergence criterion E is not met **do**
 - 5: **for all** λ_k **do**
 - 6: Calculate $\sum_{x,y} \tilde{p}(x) p_{\lambda}(y|x) f_j(x,y)$ using forward-backward algorithm
 - 7: Calculate $\sum_{k=1}^K \frac{\lambda_k^2}{2\sigma^2}$
 - 8: **end for**
 - 9: Combine Steps 3, 6, 7 (Eqn 9) and update λ using one iteration of the LBFGS Quasi Newton Method
 - 10: **end while**
 - 11: **Labeling Phase on Test Data:**
 - 12: **for all** sequences in test data **do**
 - 13: Find the labeling $y^* = \operatorname{argmax}_y P(y|x)$ for each sequence x using the Viterbi algorithm
 - 14: **end for**
-

1. In Step 1, the parameters are initialized including $\langle \lambda_j \rangle$, the convergence criterion parameter E (which determines when the Quasi-Newton method will terminate) and the regularization parameter σ^2 .
2. In Step 4, the empirical expected value of each feature f_j is calculated. This has to be done once for the training data. The cost of this step is $O(KNT)$, where K is the number of parameter, N is the number of training samples and T is the average length of the training sequences.
3. In Step 6, the expected value of each f_j under the model distribution is calculated for each training sample. This step requires the use of the forward backward algorithm [6, 26]. The total cost of this step (for all features) is $O(KNTL^2)$ where K , N and T are as before and L is the number of labels (two in our case).
4. In Step 9, the λ parameter is updated using the LBFGS Quasi Newton method. We have used an implementation LBFGS available under the

Riso open source project and which uses the sparse matrix operations available from the Java COLT distribution [11].

5. In Step 13, each test sequence is labeled using the Viterbi algorithm. The cost of Viterbi algorithm on each sequence of length T is again $O(TL^2)$

Training for extremely large applications, which are common in computational linguistics can be quite prohibitive as noted both by Sutton [26] and Cohn [6]. However, in our case, we had over one and a half million features but less than two hundred proteins in the training set, training time was never more than five minutes per iteration on typical modern machine⁵.

⁵Dell Latitude 410, 2GB RAM, 2GHz CPU